INTERNATIONAL JOURNAL FOR NUMERICAL METHODS IN FLUIDS
Int. J. Numer. Meth. Fluids 2009; **60**:79–93
Published online 17 July 2008 in Wiley InterScience (www.interscience.wiley.com). DOI: 10.1002/fld.1881

Fluid forces on a square cylinder in oscillating flows with non-zero-mean velocities

Chu-Chang Chen[1], Fuh-Min Fang[2,*,†], Yi-Chao Li[3], Long-Ming Huang[4] and Cheng-Yang Chung[2]

[1]*Department of Information Management, Chung Chou Institute of Technology, 6, Lane 2, Section 3, Shan-Chiao Road, Changhwa, Taiwan*
[2]*Department of Civil Engineering, National Chung Hsing University, 250, Kuo Kuang Road, Taichung, Taiwan*
[3]*Architecture & Building Research Insititute, Ministry of the Interior 200, Section 3, Beisin Road, Sindian, Taipei County, Taiwan*
[4]*Department of Soil & Water Conservation, National Chung Hsing University, 250, Kuo Kuang Road, Taichung, Taiwan*

SUMMARY

The unsteady forces on a square cylinder in sinusoidally oscillating flows with non-zero-mean velocities are investigated numerically by using a weakly compressible-flow method with three-dimensional large eddy simulations. The major parameters in the analysis are Keulegan–Carpenter number (KC) and the ratio between the amplitude and the mean velocities of the approaching flow (A_R). By varying the values of KC and A_R the resulting drag and lift of the cylinders are analyzed systematically at two selected approaching-flow attack angles (0 and 22.5°). In the case of the non-zero attack angle, results show that both the drag and lift histories can be adequately described by Morison equations. However, Morison equations fail to correctly describing the lift history as the attack angle is zero. In addition, when the ratio of A_R/KC is near the Strouhal number of the bluff-body flow, the resulting drag is promoted due to the occurrence of resonance. Based on the results of systematic analyses, finally, the mean and inertia force coefficients at the two selected attack angles are presented as functions of KC and A_R based on the Morison relationships. Copyright © 2008 John Wiley & Sons, Ltd.

Received 11 December 2007; Revised 5 June 2008; Accepted 5 June 2008

KEY WORDS: Morison equation; square cylinder; large eddy simulation

*Correspondence to: Fuh-Min Fang, Department of Civil Engineering, National Chung Hsing University, 250, Kuo Kuang Road, Taichung, Taiwan.
†E-mail: fmfang@nchu.edu.tw

Contract/grant sponsor: National Science Council in Taiwan; contract/grant number: NSC 96-2221-E-005-107

1. INTRODUCTION

The problem of unsteady fluid forces on a bluff body in an oscillating flow is an interesting engineering subject. In terms of fluid dynamics of bodies in oscillatory flows, there are some differences between the vortex motions and induced forces from steady uniform flow. By far, the forces acting on structures and the flow patterns around bluff bodies, such as oscillating bodies in a stationary or an unsteady flow and stationary bodies in an unsteady oscillating flow, have been discussed in the fields of aerospace, civil and coastal engineering. Since there are many examples of structural damages caused by such forces, extensive investigations are needed to explore the mechanism of the problems.

In the field of coastal engineering, to evaluate the load on piers of near-shore structures under wave actions, the analyses are generally performed under a simplified condition of a sinusoidal uniform flow past a two-dimensional cylinder. Since most of these studies consider the situations that the approaching flows possess zero-mean velocities, it is then interesting to explore how the cylinder load behaves when the approaching flows are associated with non-zero-mean velocities. In particular, the analysis can provide useful information for wind load designs in high-rise buildings under the action of gust wind.

Physically, as a flow passes a cylinder with a blunt shape, separation generally occurs due to the effect of negative pressure gradients. The separation lines can roll and form the so-called *Karman* vortices. Consequently, the flow around the body always behaves unsteadily, even when the approaching flow is steady and uniform. In the case of an oscillating approaching flow, the mechanism of the generated vortices can be affected by the action of approaching-flow acceleration and deceleration, and further lead to a change of the resulting force on the body. More critically, as the approaching-flow variation is periodic, the extent of the change may become significant as the approaching-flow frequency is close to the shedding frequency. Under such a condition, the extent of the mean and fluctuating loads can be promoted due to the effect of resonance.

To conduct an analysis of an unsteady flow past a cylinder experimentally is not easy. This is mainly due to the fact that the variation of the approaching flow is difficult to be accurately controlled. In contrast, the application of numerical simulations does not suffer from such technical difficulties. Accordingly, numerical analyses are performed to investigate the flow problem. In this study, the major concerns are the time histories of the drag and lift of the cylinder under various variation patterns of the approaching flow with non-zero-mean velocities. By varying the mean and amplitude velocities and the period of the approaching flow, the results can then be analyzed on a systematic basis.

2. THEORETICAL BACKGROUND

For a sinusoidal uniform flow past a cylinder, Morison *et al*. [1] proposed a set of theoretical descriptions about the histories of drag and lift forces on the two-dimensional body (per unit span-wise length) as follows:

$$F_{\mathrm{D}} = \frac{1}{2}\rho D C_{\mathrm{D}} U|U| + \rho A \tilde{C}_{\mathrm{D}} \frac{\mathrm{d}U}{\mathrm{d}t} \tag{1}$$

$$F_{\mathrm{L}} = \frac{1}{2}\rho D C_{\mathrm{L}} U|U| + \rho A \tilde{C}_{\mathrm{L}} \frac{\mathrm{d}U}{\mathrm{d}t} \quad \text{with } U(t) = U_0 + U_m \sin(2\pi t/T) \tag{2}$$

DOI: 10.1002/fld

where U_0 and U_m are, respectively, the mean and amplitude speeds of the approaching flow; T is the oscillation period; A and D are, respectively, the cross-sectional area and width of the cylinder; C_D and C_L denote the mean drag and lift coefficients; $\tilde{C}_D$ and $\tilde{C}_L$ represent the inertia coefficients of the unsteady drag and lift forces.

In the problem, an important parameter to describe the features of the sinusoidal approaching flow is the Keulegan–Carpenter number [2], defined as $KC = U_m T/D$. It has been widely used by researchers to characterize the variation pattern of the unsteady approaching flow.

3. RELATED STUDIES

There are a number of studies regarding cylinders in an oscillating flow field. Most of them concentrated on problems with zero-mean approaching-flow velocities. In the cases of zero-mean sinusoidal approaching flows, typically, Williamson [3] observed the motions of vortices around single circular cylinders and pairs of cylinders in a U-shape oscillating-flow tunnel. Together with the force measurement results, the observed flow patterns within different ranges of *KC* were used to explain how the lift and drag were influenced by cylinder proximity and the extent of approaching-flow unsteadiness. Sarpkaya [4] performed similar U-shape water tunnel experiments and the result of drag measurements on circular cylinders were used to check the validity of the Stokes–Wang analysis. Okajima *et al*. [5] measured the forces on circular and square cylinders at a zero approaching-flow attack angle in a U-tube water tank with a wide range of *KC* variation (1–90). Lam and Dai [6] applied PIV techniques to monitor the development of vortex structure of an oscillating circular cylinder in a water tank at low *KC* values. Zheng and Dalton [7] adopted a numerical method to simulate oscillating flows past a square cylinder at low *KC* values (up to 5) at two attack angles (0 and 45°) and compared the numerical predictions with the measurement results from Bearman *et al.* [8]. Nomura *et al*. [9] measured the forces on a square cylinder impinged by an unsteady jet with non-zero-mean velocities at two attack angles (0 and 22.5°). It was found that the drag history could be explained by Morison equations. Since the instantaneous flow field was not measured in the study, its effect on the resulting drag history was not discussed in more detail.

4. PROGRAM DESCRIPTION

In the study, a series of numerical simulations were conducted to explore the forces on a square cylinder in a periodically oscillating flow field. As shown in Figure 1, the problem of a sinusoidal flow past a square cylinder with a non-zero-mean velocity at a high Reynolds number ($Re = U_0 D/\nu$), typically of 10^7, is investigated. Two typical attack angles ($\theta = 0$ and 22.5°) are selected in the analysis. By varying the *KC* value and the amplitude velocity ratio ($A_R = U_m/U_0$), the resulting unsteady forces on the cylinder as well as the relationship between the forces and the surrounding flow field are analyzed to gain additional insight into the analysis of related engineering problems.

DOI: 10.1002/fld

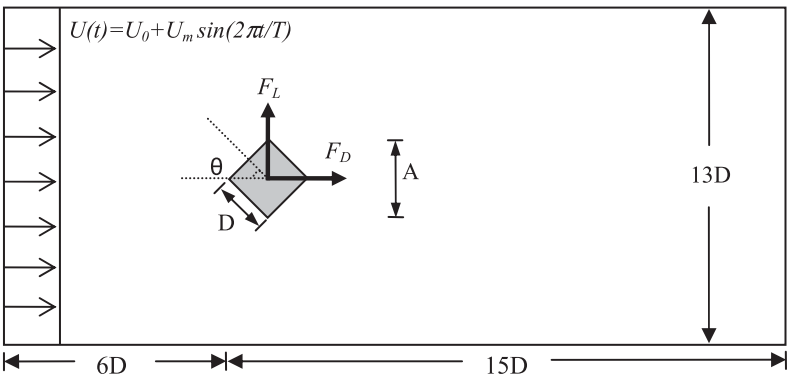

Figure 1. Sketch of the problem.

5. NUMERICAL METHOD

The simulations adopt a weakly-compressible-flow method [10] and a dynamic subgrid-scale turbulence model [11]. In the method, the continuity and momentum equations are [10]

$$\frac{\partial p}{\partial t} + k\nabla \cdot \mathbf{V} = 0 \tag{3}$$

$$\frac{\partial \mathbf{V}}{\partial t} + \mathbf{V} \cdot \nabla \mathbf{V} = -\nabla \frac{p}{\rho} + \nabla \cdot [(v + v_t)\nabla \mathbf{V}] \tag{4}$$

where p, $\mathbf{V}$ and t denote, respectively, pressure, velocity and time; k is the bulk modulus of elasticity of air. v and v_t are, respectively, the laminar and turbulent viscosities, and the latter is determined according to a dynamic subgrid-scale turbulence model proposed by Germano *et al.* [11]. Accordingly, the turbulent viscosity is obtained as

$$v_t = (C_S \Delta)^2 \sqrt{2 S_{ij} S_{ij}} \quad \text{where } S_{ij} = \frac{1}{2}\left(\frac{\partial u_i}{\partial x_j} + \frac{\partial u_j}{\partial x_i}\right) \tag{5}$$

where C_S, Δ and S_{ij} represent, respectively, the proportionality coefficient, the filter width and the strain tensor. Two filters (grid and test filters) are used to calculate C_S during the computation process. The width of the test filter is chosen as twice that of the grid filter. To avoid numerical instability due to an extensive variation of C_S in time and space, spatial averaging in the homogeneous direction is made and interpolation is used for C_S distribution between the test (coarse) and grid (fine) filters. A three-dimensional finite volume method with a collocated grid arrangement is used to solve the equations of motion. Second-order accuracy in space is used in the discretized equations of Equations (3) and (4), and the Crank–Nicolson scheme is used in time integration.

In the numerical simulations, three-dimensional flow computations are carried out in a $21\text{D} \times 13\text{D} \times 10\text{D}$ rectangular domain and the results on the middle plane in the span-wise direction of the cylinder are taken as the basis of the analysis of the two-dimensional problem. Figure 2 depicts a typical computational mesh system (266×96) on the two-dimensional (x–y) plane.

DOI: 10.1002/fld

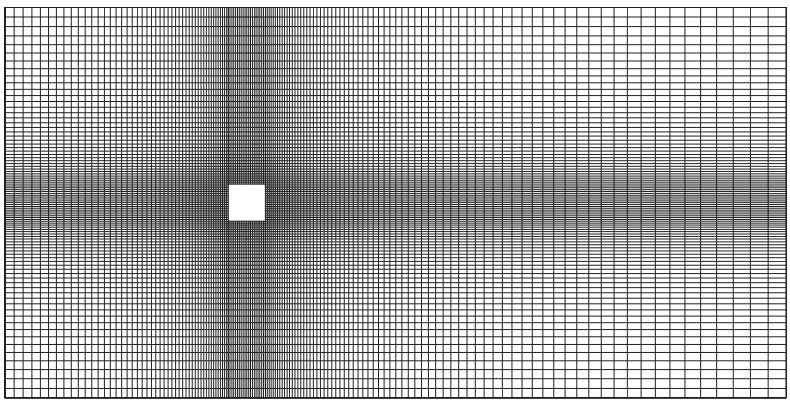

Figure 2. Typical computational mesh (266×96 grids).

Appropriate values of pressures and velocities are specified at exterior cells (or phantom cells) outside of the boundaries to reflect the physical nature of the boundaries. At the cylinder surface, a no-slip condition is used. At the side boundaries, the pressures and velocities at the phantom cells are specified according to a zero-gradient assumption in the direction normal to the boundaries. Similar zero-gradient boundary specifications are set at the span-wise end sections. At the inflow section, prescribed unsteady velocities are imposed and a zero-gradient condition is applied for pressure specifications. At the outflow boundary, on the other hand, a zero-gradient condition is used for the velocities and the sectional average pressure is set as the reference pressure of the instantaneous flow field.

6. VERIFICATIONS

To verify the accuracy of the numerical predictions, preliminary simulations of a steady uniform flow past a square cylinder at a zero attack angle are conducted. Based on the results in the middle span-wise section of three-dimensional calculations ($266 \times 96 \times 86$ grids), Table I illustrates the predicted mean and root-mean-square drag and lift coefficients as well as the Strouhal number ($St = f_s D/U_o$, f_s being the shedding frequency), compared with the experimental results by Lee [12]. It can be seen that good agreement is obtained.

It also shows in Table II that the span-wise local and averaged quantities are very close to those in the middle section. To examine the span-wise flow behavior in the same case with a steady approaching flow, Figure 3 illustrates the correlation coefficients of the velocity histories at a selected location (about 1.6D downstream of the leeward cylinder surface near the center line). The auto-correlation plot ($R_{0,0}$), associated with the middle section results, indicates that the normalized time lag cycle (8.20) is equal to the reciprocal of the Strouhal number (0.122). In addition, the cross correlations of the results between two different span-wise sections ($R_{0,-4D}$ and $R_{0,+2D}$) show that the plots are similar but with certain time lags. Accordingly, one can see that the selected span-wise domain size (10D) is large enough to describe the coherent structure of vortices in the span-wise direction.

DOI: 10.1002/fld

Table I. Comparison of predicted and experimental results of a square cylinder in steady approaching flows ($\theta = 0°$).

	Re	$\overline{C_D}$	C'_D	C'_L	St
Experimental [12]	1.76×10^5	2.05	0.22	1.22	0.12
Predicted ($266 \times 96 \times 86$ mesh)	1.76×10^5	2.046	0.223	1.213	0.122
Relative error (%)	—	0.19	1.36	0.25	1.67

Table II. Comparison of results at various span-wise cross sections.

Span-wise location (z)	Re	$\overline{C_D}$	C'_D	C'_L	St
−4D	10^7	2.043	0.220	1.212	0.121
−2D	10^7	2.044	0.222	1.213	0.122
0D (middle section)	10^7	2.045	0.222	1.213	0.122
4D	10^7	2.045	0.222	1.213	0.122
2D	10^7	2.043	0.220	1.213	0.121
−2D to 2D (average)	10^7	2.045	0.222	1.213	0.122
−4D to 4D (average)	10^7	2.044	0.221	1.213	0.122

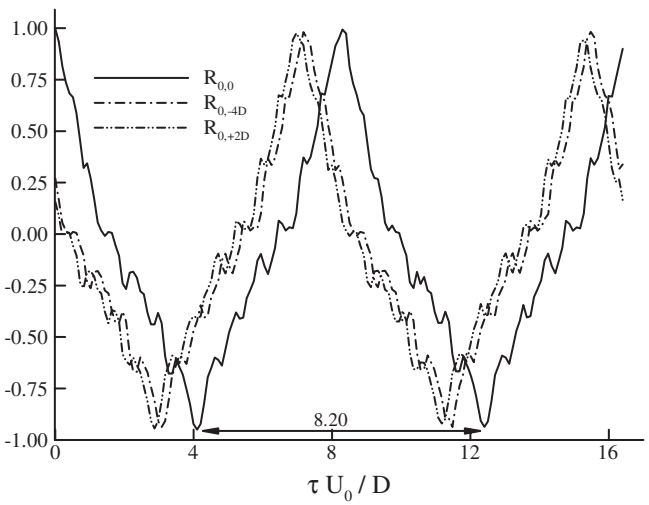

Figure 3. Correlations of lift coefficients between selected span-wise sections.

At a Reynolds number of 10^7, Table III shows the corresponding results with three mesh sizes ($186 \times 68 \times 60$, $266 \times 96 \times 86$ and $400 \times 150 \times 130$). It is found that the $266 \times 96 \times 86$ mesh is fine enough for the analysis of the problem.

DOI: 10.1002/fld

Table III. Comparison of predictions in steady approaching flows with different meshes.

Mesh	Re	$\overline{C_D}$	C'_D	C'_L	St
$186\times68\times60$	10^7	2.042	0.218	1.211	0.117
$266\times96\times86$	10^7	2.046	0.223	1.213	0.122
$400\times150\times130$	10^7	2.046	0.223	1.213	0.122

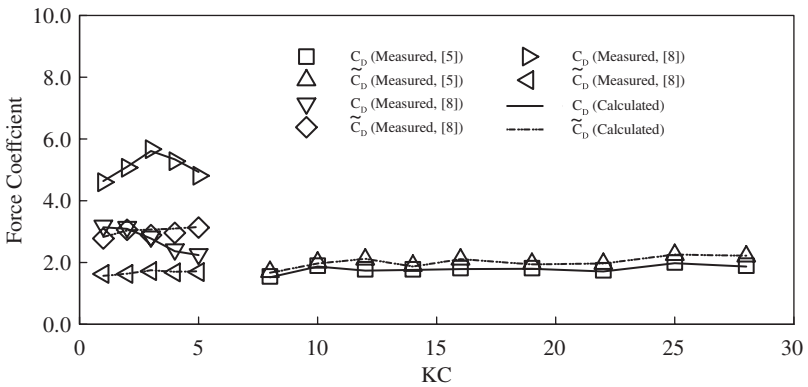

Figure 4. Comparison of force coefficients.

Table IV. Comparison of predicted and experimental results ($Re=1.4\times10^4$).

		C_D		$\tilde{C}_D$		C_L		$\tilde{C}_L$	
Attack angle	KC	Exp. [9]	Cal.	Exp. [9]	Cal.	Exp. [9]	Cal.	Exp. [9]	Cal.
0°	52	0.88	0.90	4.00	4.03	—	—	—	—
	106	0.88	0.91	4.00	4.07	—		—	—
22.5°	52	0.56	0.54	2.50	2.46	0.26	0.25	1.70	1.67
	106	0.56	0.56	2.50	2.46	0.26	0.26	1.70	1.71

Additional numerical computations are performed in certain selected cases of a square cylinder in sinusoidal approaching flows with zero-mean velocities. After obtaining the calculated drag and lift histories, the mean and inertia force coefficients associated with Morison equations are determined by performing least-square regressions according to Equations (1) and (2). Figure 4 shows the predicted force coefficients compared with the experimental results from Okajima *et al.* [5] and Bearman *et al.* [8]. The good agreement also shows the accuracy of the numerical predictions. Further calculations are carried out in the cases of Nomura *et al.* [9]. It indicates in Table IV that the results are again well predicted.

DOI: 10.1002/fld

7. RESULTS

After the applicability of the present numerical method is verified, a series of numerical calculations are then carried out at two approaching-flow attack angles ($\theta=0$ and 22.5°) for systematic analysis of the resulting drag and lift forces on the cylinder. In the program of analyses, four amplitude velocity ratios ($A_R=0.1, 0.3,$ 0.5 and 0.7) are selected with KC varying from 0.5 to 15. The selection covers a sufficiently wide range of approaching-flow variations in common engineering applications. Considering the interest of wind-engineering applications, in particular, the systematic analysis deals with the condition that the approaching flow possesses a non-zero-mean velocity and is free of flow reversal to reflect the general behavior of wind.

Typically, in the case of a zero attack angle ($A_R=0.5$ and $KC=4$), Figure 5 shows the calculated normalized iso-vorticity contours within a period of approaching-flow variation. One can see that the motion of the generated vortices is significantly influenced by the inertia effect of the approaching flow. When the approaching flow is subject to acceleration, the vortices are pushed towards downstream and the wake region appears stretched. During the period of deceleration, on the other hand, the movement of the vortices appears delayed, resulting in a wider wake region compared with that of *Karman* vortices in a steady approaching flow.

Figure 6 depicts the history of the resulting normalized drag together with the theoretical relationship of Equation (1). The comparison shows that the Morison equation (Equation (1)) well describes the time variation of drag. In contrast, the comparison of the corresponding lift history (Figure 7) with Equation (2) shows that the Morison relationship (Equation (2)) describes the lift variation poorly. As θ equals to a non-zero value (22.5°), Figures 8 and 9 again show that the corresponding drag and lift histories are adequately described by Morison equations.

On the basis of the series of numerical results, Figure 10 depicts the mean and inertia drag coefficients (C_D and $\tilde{C}_D$) as functions of KC at various A_R values in the case of a zero attack angle. Generally, the variation of C_D starts with a small quantity then increases to a peak value as the ratio of A_R/KC (physically being the normalized oscillation frequency of the approaching flow) is close to that of the Strouhal number corresponding to the steady approaching-flow case. As KC increases further, C_D decreases and finally tends to a constant value, which is equal to the mean drag coefficient ($\overline{C_D}$) associated with the steady approaching-flow case. In contrast, the inertia drag coefficient decreases with an increase of KC. As KC becomes rather large, $\tilde{C}_D$ tends to zero.

Regarding the effect of the amplitude velocity ratio (A_R), Figure 10(a) shows that when A_R increases, the corresponding peak value of C_D also increases. Meanwhile, the condition that C_D approaches to the steady value occurs at a relatively larger KC value. Moreover, the result in Figure 10(b) indicates that a larger A_R generally leads to a greater value of $\tilde{C}_D$.

In the case of the non-zero attack angle ($\theta=22.5^\circ$), on the other hand, Figures 11 and 12 illustrate the results of the corresponding mean and inertia force coefficients. It can be seen that the variation patterns of both the drag and lift coefficients are similar to those of the drag coefficient variations (Figure 9(a)) in the zero attack angle case.

8. DISCUSSION

Considering the fact that investigating the problem of an unsteady flow past a cylinder experimentally is not easy, numerical analyses are performed in the study to analyze the flow effect of

DOI: 10.1002/fld

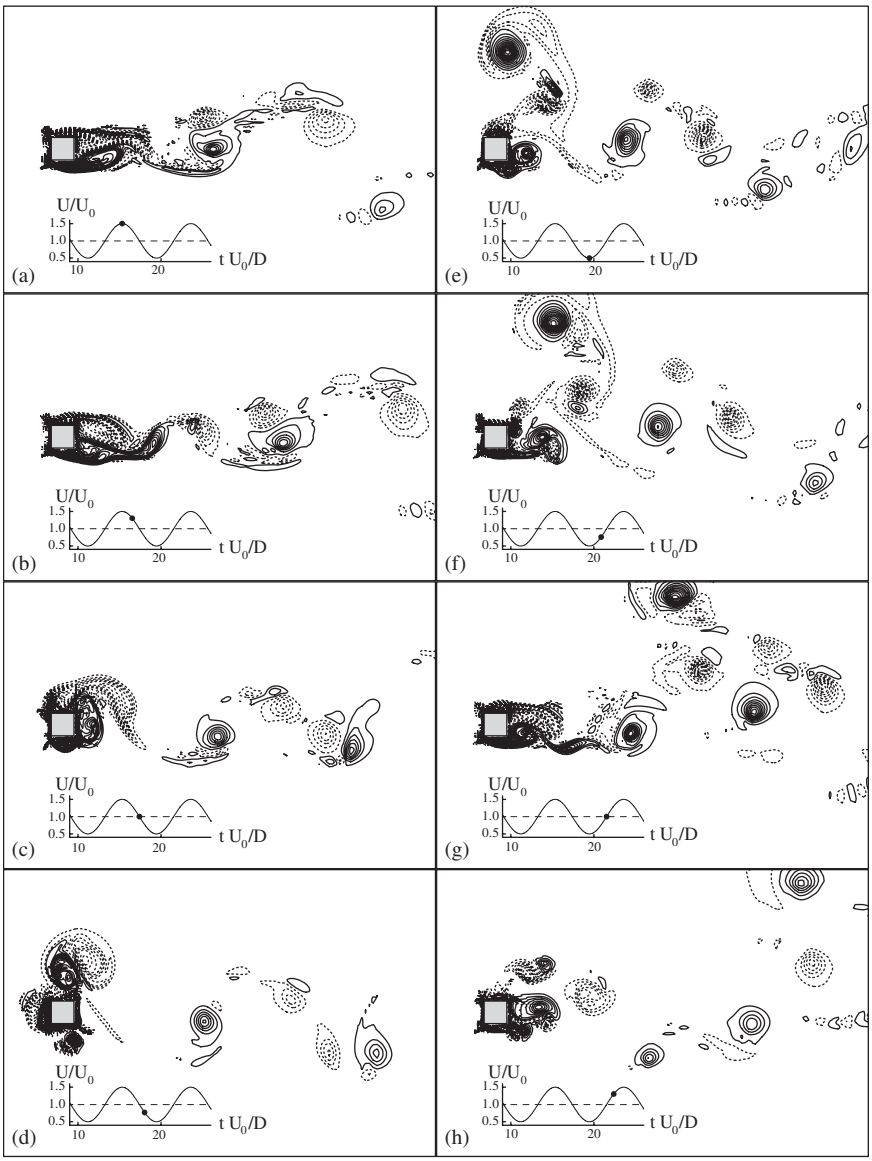

Figure 5. Instantaneous iso-vorticity contours within a period of approaching-flow variation ($\theta = 0°$, $A_R = 0.5$ and $KC = 4$).

the cylinder on a systematic basis. By comparing the numerical predictions with the measurement results, good agreements in steady approaching-flow cases (Table I) and oscillating approaching-flow cases with zero-mean velocities (Figure 4 and Table IV) indicate the validity and accuracy of the present three-dimensional large eddy simulations (LESs) in predicting the behavior of flow around a square cylinder impinged by an oscillating approaching flow.

DOI: 10.1002/fld

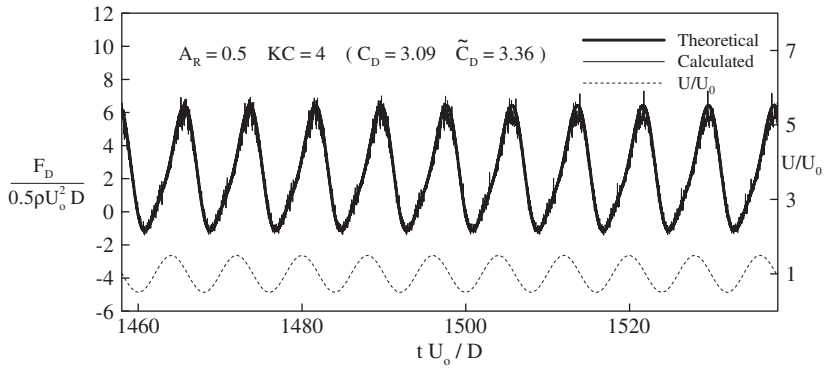

Figure 6. Comparison of normalized drag histories ($\theta = 0°$).

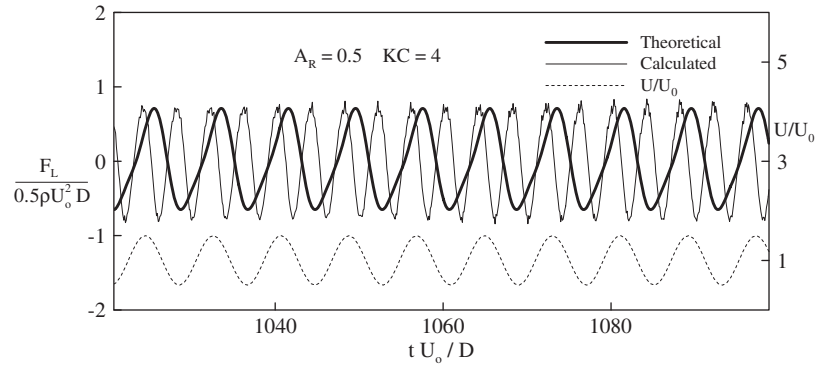

Figure 7. Comparison of normalized lift histories ($\theta = 0°$).

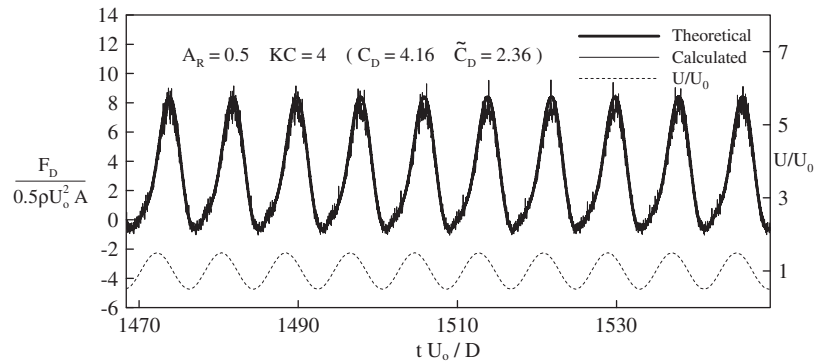

Figure 8. Comparison of normalized drag histories ($\theta = 22.5°$).

DOI: 10.1002/fld

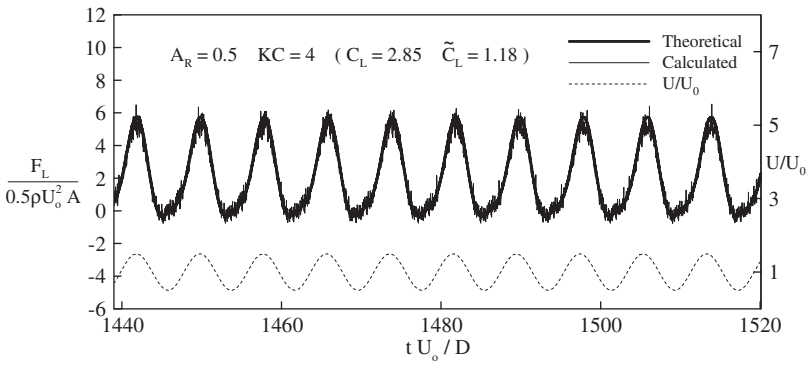

Figure 9. Comparison of normalized lift histories ($\theta = 22.5°$).

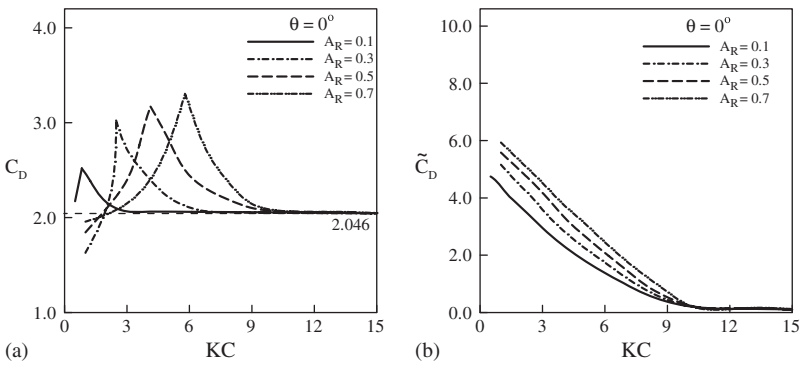

Figure 10. Variations of mean and inertia drag coefficients based on Morison equations ($\theta = 0°$).

Physically, Keulegan–Carpenter number can be regarded as the ratio between the translation of a fluid particle within a period of T and the transverse dimension of the cylinder [2]. Difficulty is encountered, however, as KC is used to reflect the extent of approaching-flow unsteadiness in the analysis. For example, one KC value can be the outcome of either a large U_m with a small T or a small U_m with a large T, which correspond to two significantly different approaching-flow conditions. Accordingly, the amplitude velocity ratio ($A_R = U_m / U_0$) is proposed to be the second parameter in the study to characterize the variation of the approaching flow more specifically. Once A_R is determined, a larger KC then indicates that the extent of the approaching-flow unsteadiness becomes milder. Consequently, the program of the systematic analyses can then proceed in a more convenient way.

The result of the instantaneous normalized iso-vorticity contours (Figure 5) in the typical case ($\theta = 0°$, $A_R = 0.5$ and $KC = 4$) appears quite interesting. The approaching-flow acceleration and deceleration apparently affect the vortex motion, leading to deviation of the wake pattern from that of common *Karman* vortices. Further calculations of the numerical results show that the mean drag coefficient is 2.272. Compared with that in the steady approaching case (2.046; see Table III), it reveals that the unsteadiness of the approaching flow tends to increase the mean drag force.

DOI: 10.1002/fld

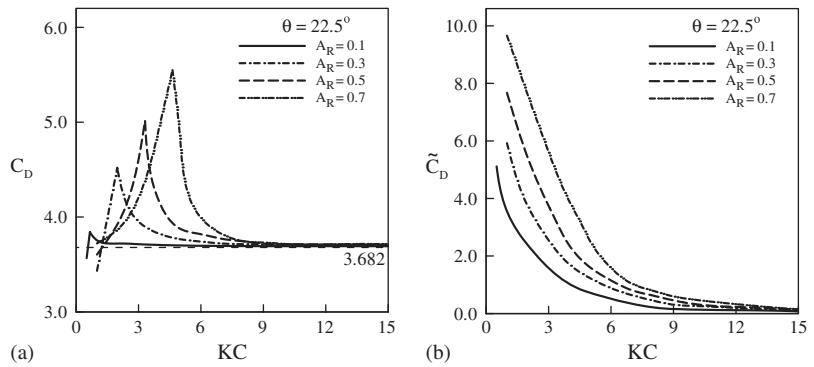

Figure 11. Variations of mean and inertia drag coefficients based on Morison equations ($\theta = 22.5°$).

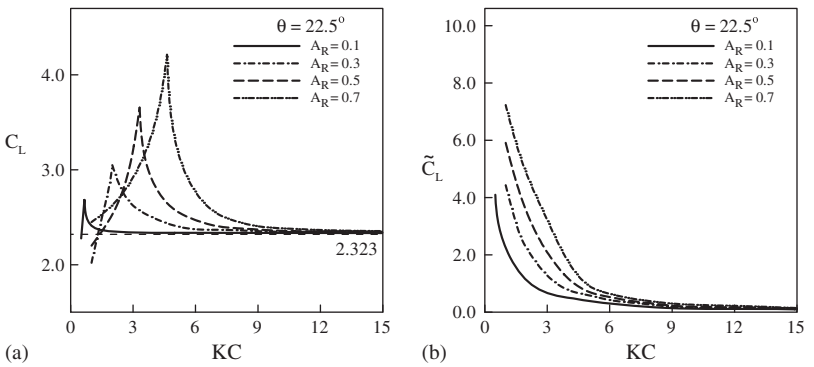

Figure 12. Variations of mean and inertia lift coefficients based on Morison equations ($\theta = 22.5°$).

By performing least-square regressions, it shows typically in Figures 6 and 8 that the drag histories at the two approaching-flow attack angles are well described by the Morison relationship (Equation (1)). However, examinations on the lift histories (Figures 7 and 9) reveal that Equation (2) fails to describe the lift history correctly when the approaching-flow attack angle is zero (Figure 7). This agrees with what has been found in the previous studies [7–9]. Physically, the lift force is determined based on the surface pressures on both sides of the cylinder when the attack angle is zero. Since the cylinder sides are not directly impinged by the approaching flow, the cylinder can hardly experience the inertia effect. This can explain why the theory of Morison equations cannot properly describe the resulting lift variation when the attack angle is zero. For the same reason, the frequencies of the lift histories in Figures 7 and 9 appear different.

The examples in Figures 6–9 show that there are some wiggles in the resulting drag and lift histories. Similar types of results are also found in the measurements by Nomura *et al*. [9]. Further examinations on the differential values between the calculated and theoretical results were carried out. The shapes of all the resulting spectra (Figure 13), similar to that of white noise, reveal that these wiggles may be attributed to the outcome of turbulence. To support this conclusion, however, additional extensive experimental investigation will be needed.

DOI: 10.1002/fld

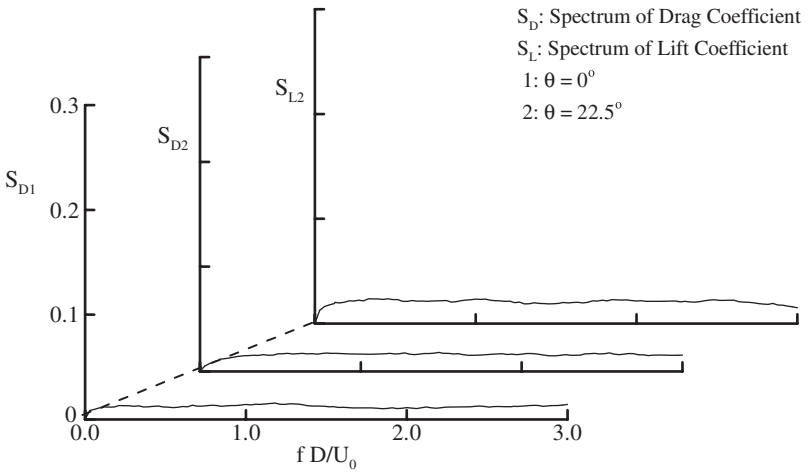

Figure 13. Power spectra of drag and lift coefficients.

The general pattern of C_D variations seems also interesting, as depicted in Figures 10(a) and 11(a). The same tendency is also detected on the C_L variation at a non-zero attack angle (Figure 12(a)). Mathematically, it can be shown that the ratio of A_R/KC represents the normalized oscillation frequency of the approaching flow. As this ratio is near the Strouhal number of the bluff-body flow, the mean drag coefficient (C_D) is greatly promoted. Consequently, C_D reaches a peak value due to the occurrence of resonance. In addition, the resulting peak values of C_D (Figures 10(a) and 11(a)) and C_L (Figure 12(a)) increase with an increase of A_R, implying that the extent of resonance effect is enhanced when the amplitude velocity of the approaching flow becomes greater. Moreover, when KC is sufficiently large, the extent of the approaching-flow unsteadiness becomes weaker, leading to the result that C_D (or C_L) tends to the $\overline{C_D}$ (or $\overline{C_L}$) value, corresponding to the steady approaching-flow case.

Figures 10(b)–12(b) show that the tendencies of $\tilde{C}_D$ and $\tilde{C}_L$ variations are different from those of C_D and C_L. Since $\tilde{C}_D$ and $\tilde{C}_L$ are related, respectively, to the inertia part of drag and lift, they do not appear to be affected by the occurrence of resonance. As a result, $\tilde{C}_D$ and $\tilde{C}_L$ start with large values then decrease rapidly as KC increases and eventually tend to zeros.

Based on the numerical results, finally, Figure 14 illustrates typically ($A_R = 0.3, \theta = 0°$) the resulting mean and inertia coefficients as a function of KC. One can see that as Re exceeds 10^5, the results are insensitive to the change of Reynolds number.

9. CONCLUSION

The unsteady forces on a square cylinder in sinusoidally oscillating flows with non-zero-mean velocities at a zero and a typical non-zero (22.5°) attack angles are investigated numerically. Preliminary numerical tests have shown that the present three-dimensional LES method can be applied to obtain the predicted results with an acceptable accuracy. By varying Keulegan–Carpenter number (KC) and the amplitude velocity ratio (A_R), which are used to characterize the unsteady

DOI: 10.1002/fld

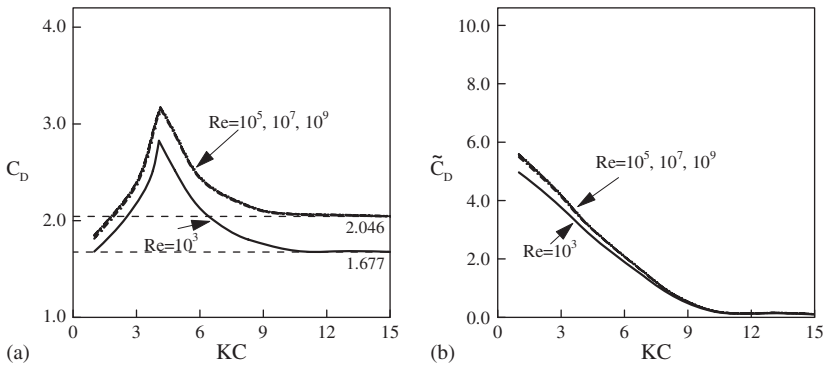

Figure 14. Comparison of mean and inertia drag coefficients at different Reynolds numbers.

pattern of the approaching-flow variation, the resulting forces on the cylinders are analyzed systematically. Based on the results of numerical simulations, several conclusions are drawn as follows:

1. In the case of a zero attack angle, Morison equations can adequately describe the resulting drag history but fail to correctly describe the lift history.
2. When the attack angle is non-zero, the Morison relationships can well describe both the resulting drag and lift histories.
3. With a fixed value of A_R, the variation of the mean drag coefficient (C_D) starts with a small quantity then increases to a peak value as the ratio of A_R/KC is near that of the Strouhal number corresponding to the steady approaching-flow case. As KC increases further, C_D decreases and finally tends to the value of the mean drag coefficient in the steady approaching flow case. In contrast, the inertia drag coefficient ($\tilde{C}_D$) decreases with an increase of KC. As KC becomes rather large, $\tilde{C}_D$ tends to zero.
4. As the ratio of A_R/KC is near the Strouhal number of the cylinder in the steady case, the mean drag is promoted due to the resonance effect. The extent of enhancement becomes greater as KC increases.
5. In the case of a non-zero attack angle, the inertia drag coefficient ($\tilde{C}_D$) decreases with an increase of KC and is not affected by the occurrence of resonance. As KC becomes rather large, $\tilde{C}_D$ tends to zero.
6. The mean and inertia drag coefficients at the two selected attack angles (0 and 22.5°) are presented as functions of KC and A_R. The presented relationships, which are insensitive to a Reynolds number greater than 10^5, can be applied to evaluate the force acting on structures with a square cross section under the action of oscillating approaching flows with non-zero mean velocities.

ACKNOWLEDGEMENTS

The study was cordially funded by the National Science Council in Taiwan (grant no. NSC 96-2221-E-005-107).

DOI: 10.1002/fld

REFERENCES

1. Morison JR, O'Brien MP, Schaaf SA, Johnson JW. The force exerted by surface waves on piles. *Petroleum Transactions*, *AIME* 1950; **189**:149–157.
2. Keulegan GH, Carpenter LH. Forces on cylinders and plates in an oscillating fluid. *Journal of Research of the National Bureau of Standards* 1958; **60**:423–440.
3. Williamson CHK. Sinusoidal flow relative to circular cylinders. *Journal of Fluid Mechanics* 1985; **155**:141–174.
4. Sarpkaya T. Force on a circular cylinder in viscous oscillatory flow at low Keulegan–Carpenter numbers. *Journal of Fluid Mechanics* 1986; **165**:61–71.
5. Okajima A, Matsumoto T, Kimura S. Force measurements and flow visualization of circle and square cylinders in oscillatory flow. *JSME International Journal* 1998; **41**:796–805.
6. Lam KM, Dai GQ. Formation of vortex street and vortex pair from a circular cylinder oscillating in water. *Experimental Thermal and Fluid Science* 2002; **26**:901–905.
7. Zheng W, Dalton C. Numerical prediction of force on rectangular cylinders in oscillating viscous flow. *Journal of Fluids and Structures* 1999; **13**:225–249.
8. Bearman PW, Graham JMR, Obasaju ED, Drossopoulos GM. The influence of corner radius on the forces experienced by cylindrical bluff bodies in oscillatory flow. *Applied Ocean Research* 1984; **6**:83–89.
9. Nomura T, Suzuki Y, Uemura M, Kobayashi N. Aerodynamic forces on a square cylinder in oscillating flow with mean velocity. *Journal of Wind Engineering and Industrial Aerodynamics* 2003; **91**:199–208.
10. Song CCS, Yuan M. A weakly compressible flow model and rapid convergence methods. *Journal of Fluids Engineering—Transactions of the ASME* 1988; **110**:441–455.
11. Germano U, Piomelli P, Cabot WH. A dynamic subgrid-scale eddy viscosity model. *Physics of Fluids* 1991; **3**:1760–1765.
12. Lee BE. The effect of turbulence on surface pressure field of a square prism. *Journal of Fluid Mechanics* 1975; **69**:263–282.

DOI: 10.1002/fld